First publ. in: Journal of Chemical Physics 91 (1989), 12, pp. 7972-7977

Photoionization thresholds of rare gas clusters

G. Ganteför,[a] G. Bröker, E. Holub-Krappe, and A. Ding
Bereich Strahlenchemie, Hahn-Meitner Institut, 1000 Berlin 39, Germany

Photoionization efficiency curves of rare gas clusters generated by supersonic expansion of pure argon, krypton, and xenon gas have been measured as a function of photon energy using light from the Berlin Electron Synchrotron Facility (BESSY). Assuming that the relative shapes of the efficiency curves are independent of cluster size, ionization potentials for each cluster can be extracted from the data by using the known absolute ionization thresholds of the dimer or trimer ions. The data agree with the model that ionic clusters are composed of an ionic substructure surrounded by shells of atoms. In particular, it has been confirmed that Ar_3^+ is the central substructure in Ar_n^+ for $n < 15 \pm 1$. In addition we have estimated the ratio of the covalent binding energy to the charge-induced dipole binding energy for the ions. The larger dipole-induced binding energy in the case of xenon may explain the differences between the mass spectra of Xe and Ar clusters.

I. INTRODUCTION

One important reason for the rapid development of cluster physics in the last decade is the discovery of "magic numbers" in the mass spectra of clusters. These were demonstrated for the first time in the case of Xe clusters[1]; the mass spectra clearly showed size dependent intensity fluctuations, which are explained by the differing stabilities of the neutral clusters. It was concluded that clusters form icosahedral structures[2] consisting of an atom in the center surrounded by shells of atoms. Particularly stable are those structures which consist of completely filled shells, because the mean number of nearest neighbors per atom, and therefore the bond strength, is a maximum for such a geometry. On the other hand, an additional atom attached to a closed shell can be only loosely bound as the coordination number cannot exceed three. The shell closings are expected at $n = 13$, 19, 55, 147, 548,.... Most of those appear in mass spectra of ionized Xe_n^+ clusters.[3]

These simple considerations do not hold for ionic systems. Clusters (and also molecules) change their geometry after ionization because of the influence of the charge.[4] Change in cluster geometry upon ionization causes a release of internal energy initiating severe fragmentation in the case of van der Waals clusters.[5–10] This leads to mass distributions of ionic clusters which deviate significantly from the predicted size distributions of the neutral clusters.[11] The fluctuations observed in the mass spectra thus reflect simultaneously the dynamics of the fragmentation mechanism, the stabilities of the cluster ions, and the size distribution of the neutrals. For example, it has been found that mass spectra of Ar_n^+ clusters differ significantly from those of Xe_n^+ obtained by the same experimental techniques[11] (e.g., no maximum found for Ar_{13}^+; the intensity of Ar_{21}^+ is larger than that of Ar_{19}^+). Likewise, the deviations observed in mass spectra of Ar_n^+ clusters produced by condensation of neutral atoms around Ar^+ or Ar_2^+ are still without explanation.[12]

During the past years a number of different experimental approaches have been used applying mass spectrometry and coincidence techniques to investigate the role of fragmentation.[5–8,13] Different theoretical models have been tried in an attempt to explain the experiments.[4,9,10,14] It has been suggested that the cluster ions consist of a chemically bound ionic substructure to which the additional atoms are attached by ion-induced dipole forces.[4,15,16] In the case of homogeneous rare gas cluster ions, it had been postulated that these substructures consists of dimer ions.[4] Recent theoretical[15,17] and experimental[18] investigations suggest, however, that these substructures are trimer and tetramer ions which also display strong chemical bonding. In this paper we will show that our data may indeed be explained with the use of the trimer ion model.

II. EXPERIMENTAL METHOD

We use the photoion–photoelectron coincidence method as described in detail in earlier publications[19,20] for the measuring of the ionization thresholds of rare gas clusters. The neutral clusters are produced by supersonic expansion of the pure rare gas through a 30 μm nozzle at room temperature. The stagnation pressure (Ar: 15 Bar; Kr: 5 Bar; Xe: 4 Bar) is optimized to produce cluster ions in the size region of interest. After passing a skimmer the cluster beam crosses the focus of a monochromatic VUV light beam, delivered by the Berlin Electron Synchrotron Facility (BESSY). Typical photon fluxes of about 10^{10} photons/s are available at ~ 3 Å resolution in a photon energy range of 10–20 eV. A homogeneous electrical field parallel to the cluster beam axis accelerates the cluster photoions downstream. After passing a drift region they reach a channel plate detector. Photon energy-dependent mass spectra are obtained by the time-of-flight (TOF) method. Low-energy photoelectrons serve to initiate the time measurement. The advantage of the TOF method as compared to the use of a quadrupole mass analyzer is the simultaneous measurement of the entire cluster spectrum. Correct design of the arrange-

[a] Fakultät für Physik, Universität Beilefeld, 48 Bielefield 1, Germany.

ment of fields and electrodes yields a mass resolution of about $m/\Delta m = 500$, if thermal broadening is negligible. From an analysis of mass spectra obtained at different photon energies we determine the ionization potentials (IP's) as described in detail below.

III. EXPERIMENTAL RESULTS AND DATA ANALYSIS

TOF spectra has been taken at different photon energies. Figure 1 shows as examples three rare gas cluster mass spectra. The photon energies have been chosen such as to obtain a high cluster signal. Distinct differences between Xe- and Ar-cluster spectra are obvious and in agreement with other measurements.[11] A principal problem of the coincidence method is the background counts produced by random coincidences. It limits the dynamical range of the observed line intensities and considerably prolongs measurements near the threshold. The time for obtaining a single mass spectrum of sufficient quality varies from 15 min to 10 h depending on the photon energy.

For the extraction of ionization thresholds from such spectra an elaborate numerical treatment is necessary. First the background is subtracted and the area of every mass peak is integrated. The line areas are normalized to the corresponding monomer peaks as the monomer ions are produced in this photon energy range (Ar: 14–15 eV) by light from the second order of the monochromator. The ionization cross section of argon atoms around 28–30 eV is nearly independent of photon energy[21]; the intensity must, therefore, be independent of wavelength and can be used for calibration. This method has turned out to be superior to the normalization to the integrated light flux. As we are interested in the dependence of the relative ionization cross section on the photon energy only, we normalize the intensities at one suitable energy. While lowering the photon energy the intensity change is observed.

The resulting spectra are shown in Fig. 2 for argon. At reduced ionization energy the small clusters are the first to display a strong loss of intensity. The mass distribution shifts

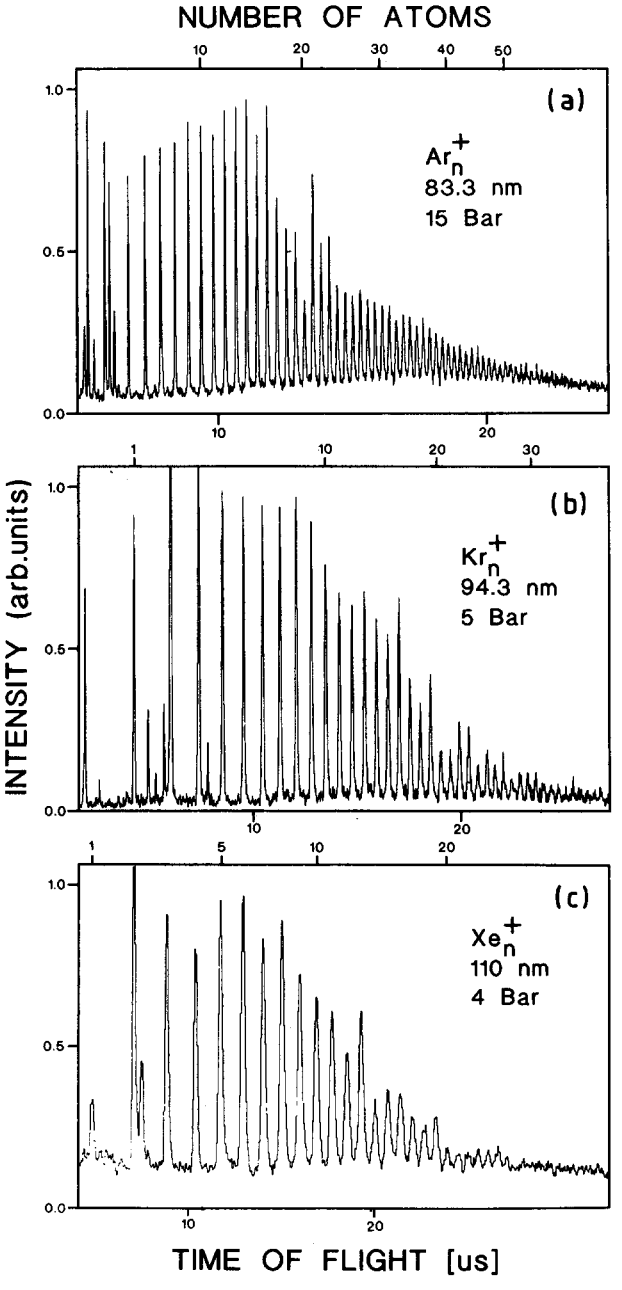

FIG. 1. Time of flight mass spectra of Ar_n^+ (a), Kr_n^+ (b), and Xe_n^+ (c) cluster ions obtained by photoionization of neutral clusters condensed in a pure rare gas expansion. Photon energies have been chosen to produce high cluster intensities.

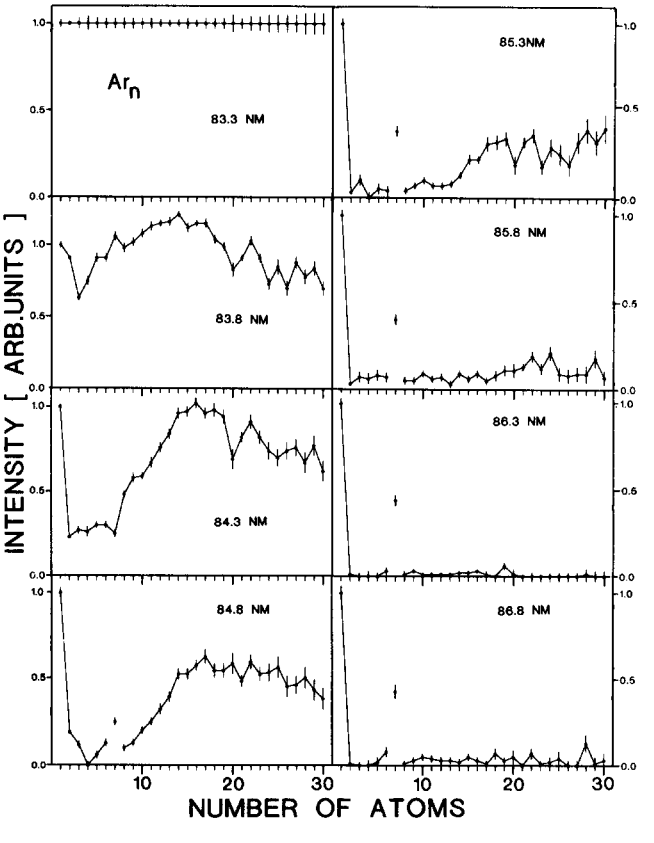

FIG. 2. Peak areas of argon cluster ions obtained at eight different photon energies. The intensities in each spectrum are normalized to the monomer line which exhibits no dependence on photon energy. In order to remove the intensity variation with n all values at 14.98 eV are assumed to be unity. The line near Ar_7^+ is caused by background impurities.

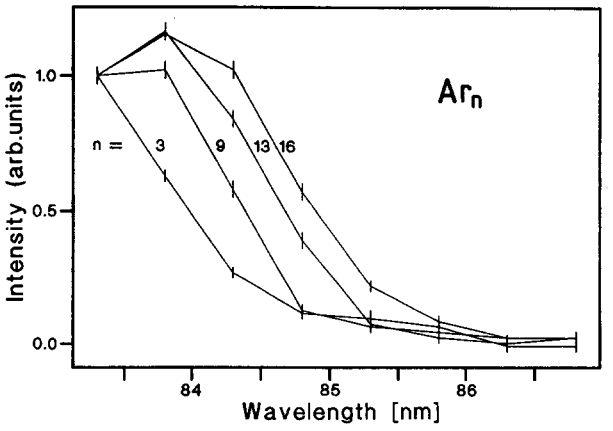

FIG. 3. Line intensities from Fig. 2 as a function of wavelength for four different lines.

to larger n until most of the lines vanish. For small n ($\leqslant 15$) the ionization thresholds vary gradually with n. This corresponds to a "red shift" of the ionization efficiency curves from $n = 3$ to $n \approx 15$. The larger clusters exhibit nearly identical ion efficiency curves. The exceptionally high intensity at the position of Ar_7^+ (see Fig. 2) at low photon energies is produced by photoionization of an impurity with nearly the same mass as Ar_7^+.

A different representation of the data is given in Fig. 3. The normalized line intensities of selected clusters are plotted vs the wavelength. The efficiency curves show a distinct wavelength dependence but are very similar. If we assume equal relative shapes for all cluster sizes we are able to approximate somewhat arbitrarily the shift of the IP's by evaluation of the half maximum ion intensities. These relative shifts can be calibrated to the adiabatic IP of Ar_3 which is the largest one with known IP. The IP of Ar_3 (14.34 eV) is calculated from the IP of the monomer (15.755 eV),[22] the dissociation energies of the neutral dimer (0.012 eV)[22] and trimer (estimated as two times the dimer = 0.024 eV) and the dissociation energies of the ionic dimer (1.25 eV)[22] and ionic trimer (0.2 eV).[23] Figure 4(a) shows the IP's of Ar_n for $n = 2,...,20$. Note that we determined the adiabatic IP assuming a constant difference between the vertical and the

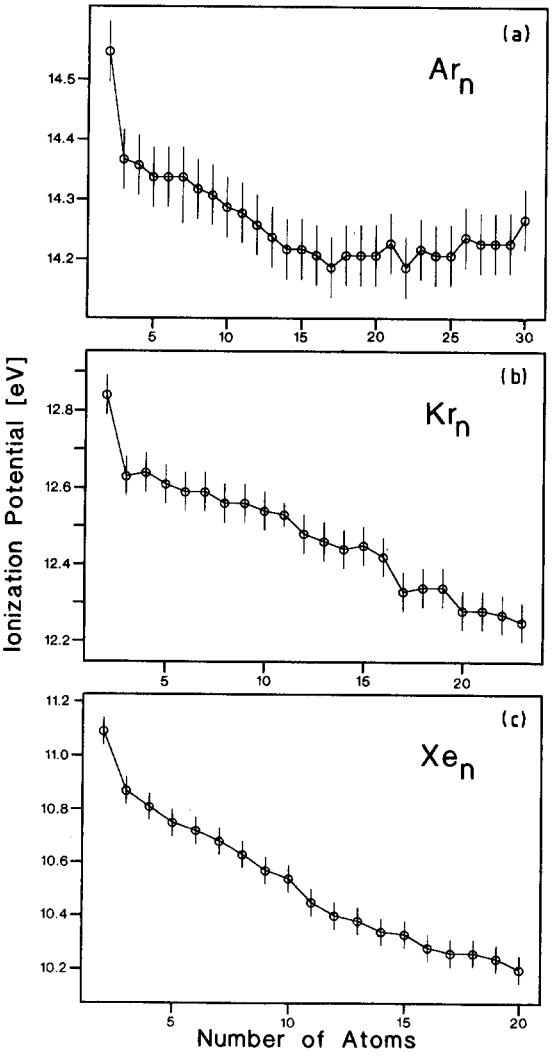

FIG. 4. Ionization potentials of argon(a), krypton(b), and xenon(c) clusters. The values of Ar_3 (Refs. 22 and 23), Kr_2 (Ref. 24), and Xe_3 (Ref. 25) serve as a calibration of the measured relative IP's shifts.

TABLE I. The ionization potentials obtained from the ion efficiency curves. The uncertainty of each value is ± 0.05 eV with the exception of that of Ar_7 ($^{+0.05}_{-0.07}$ eV). An additional error is caused by the calibration of the whole sequence by the known data of the trimers or dimers and the uncertainty of the assumption of equal efficiency curves particular for small clusters. The overall error might be around ± 0.1 eV. Data from literature are marked by the reference numbers.

	Ionization potentials (eV)		
n	Ar	Kr	Xe
1	15.75[a]	14.00[a]	12.13[a]
2	14.52[a]	12.88[c]	11.09[a]
3	14.34[a,b]	12.63	10.88[d]
4	14.36	12.64	10.81
5	14.34	12.61	10.75
6	14.34	12.59	10.72
7	14.34	12.59	10.68
8	14.32	12.56	10.63
9	14.31	12.56	10.57
10	14.29	12.54	10.54
11	14.28	12.53	10.54
12	14.26	12.48	10.40
13	14.24	12.46	10.38
14	14.22	12.44	10.34
15	14.22	12.45	10.33
16	14.21	12.42	10.28
17	14.19	12.33	10.26
18	14.21	12.34	10.26
19	14.21	12.34	10.24
20	14.21	12.28	10.20
21	14.23	12.28	
22	14.19	12.27	
23	14.22	12.25	
24	14.21		
25	14.21		
26	14.24		
27	14.23		
28	14.23		
29	14.23		
30	14.27		
∞	13.9[a]	11.9[a]	9.7[a]

[a] Reference 22.
[b] Reference 23.
[c] Reference 24.
[d] Reference 25.

adiabatic IP (= identical shapes of the efficiency curves).

The IP's of Ar_n change from Ar (15.755 eV)[22] to Ar_3 (14.34 eV) by about 1.4 eV. From $n = 3$ to $n \approx 15$ the further change amounts only to ~0.2 eV with a final difference of ~0.3 eV to the bulk work function (13.9 eV).[22] The IP's show a nearly constant decrease with increasing cluster size until $n \approx 15$ and then remain constant within the resolution of our experiment. The IP's of krypton and xenon clusters determined in an analogous manner are shown in Figs. 4(b) and 4(c). The IP's of Kr_n are calibrated to the value of the dimer (12.88 eV),[24] those of Xe_n to the trimer IP (10.88 eV).[25] Table I gives a compilation of all measured IP's. The ion efficiency curves of clusters composed of these heavier rare gases are not as smooth as those of the argon plots. In some cases we found pronounced resonances near the threshold.

The IP's of krypton and xenon clusters show a smooth variation with cluster size and exhibit no change in slope as in the case of argon. From a comparison of the three pictures of Fig. 4 information can be extracted about the bond structure of the rare gas cluster ions which will be discussed in the following section.

IV. DISCUSSION

Ionization potentials are related to the total binding energies of the neutral and the corresponding positive clusters as illustrated in Fig. 5. The total binding energy is defined as the energy which is needed to separate a neutral cluster into single atoms or a cluster ion into a positive ion, an electron and the residual atoms. The absolute energy is not relevant for our considerations. We begin with the levels which are

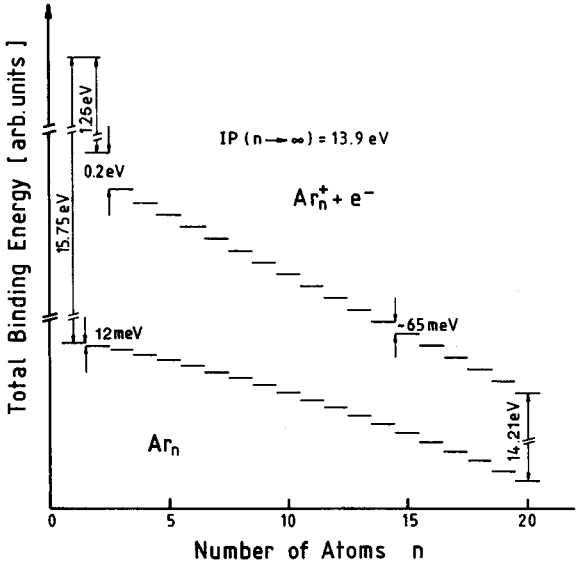

FIG. 5. Schematical diagram of the total binding energy of neutral Ar_n clusters and Ar_n^+ cluster ions (for details see text). The values of the atomic IP, the binding energies of Ar_2^+ and Ar_2 and the argon bulk work function are taken from Ref. 22; the IP of Ar_{20} is from this work. The binding energy of an atom to a neutral Ar_{15} is a rough estimate based on geometrical considerations and that of an atom to a charged Ar_{15}^+ is a theoretical value (Ref. 15).

connected by the IP of 15.75 eV. The dimer IP is significantly lower because the binding energy of Ar_2^+ (1.25 eV)[22] is much higher than that of the neutral Ar_2(0.012 eV).[22] The addition of another atom to form Ar_3^+ (0.2 eV)[23] lowers the IP of Ar_3 further to 14.34 eV.

The gain in binding energy for the neutrals caused by the addition of an atom (lower series in Fig. 5) increases with n according to the increase of the number of nearest neighbors. The bulk limit is 80 meV/atom[22] corresponding to a coordination number of 12 (fcc structure). In the case of small ionic clusters an additional atom is bound to the central charge by the induced dipole interaction. The interaction is distance dependent and one expects a significant influence on atoms in the neighborhood of the charge only. For atoms bound to the surface of large clusters the same binding energy is therefore expected for charged and neutral ones. Thus both series of levels in Fig. 5 must converge with increasing n to parallel slopes of 80 meV/atom at a relative distance of 13.9 eV (bulk work function).[22]

With the aid of Fig. 5 we can qualitatively understand the data displayed in Fig. 4(a), (b), (c). The striking drop of the IP's going from $n = 1$ to $n = 3$ is caused by the covalent bond of the dimer and trimer ions. The further decrease reflects the induced dipole interaction, which causes a stronger binding of additional atoms to small ionic clusters compared with neutrals. In the case of argon this slope becomes horizontal at about $n \approx 15$ and the IP's of the heavier clusters do not change significantly. This implies an equal binding energy of additional atoms independent of the charge of the cluster. A recent experiment on neutral and ionic dissociation energies led to a similar conclusion for $n \geqslant 20$ or possibly smaller clusters.[18] We conclude that the central charge is already completely screened by the first coordination shell.

In a pure Makay icosahedron[2] the closing of the first coordination shell is expected at $n = 3$. If we assume the charge to be located on a linear trimer Ar_{13}^+ could be an icosahedron with the trimer as one axis. Then two more bonding sites exist as next neighbors to the charge at the ends of the trimer.[17] This may shift the shell closing towards $n = 15$ for Ar_n which is consistent with the data in Fig. 4. There exist ten additional less favorite sites arranged around the trimer ends, which lead to a further shell closing at $n = 25$.[17] These 10 atoms are weaker bound than those which are in direct "touch" to the trimer ion.

The data of krypton and xenon in Fig. 4 show no signs of the closing of the first coordination shell. The reason may be due to the higher polarizability of the larger rare gas atoms. A higher polarizability implies a higher positive charge on the surface of the shell and so a less effective screening. It is conceivable that a kink might be observed when the second coordination shell is completed ($n = 55$).

For a direct comparison of the IP's convergence against their respective bulk values Fig. 6 displays the normalized differences between cluster IP's and bulk work function. From this figure one can get some insight into the relaxation effects in the bulk, which cause the lowering of the bulk work function compared to the atomic IP. The main contribution in the case of argon (~80%) stems from the covalent bind-

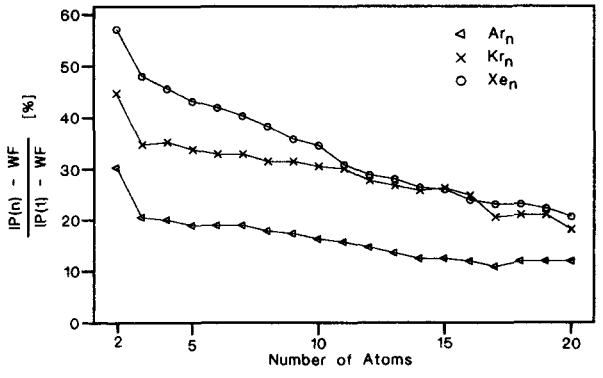

FIG. 6. The relative deviation of the cluster IP's from the bulk work function taking the value of the atom as 100%.

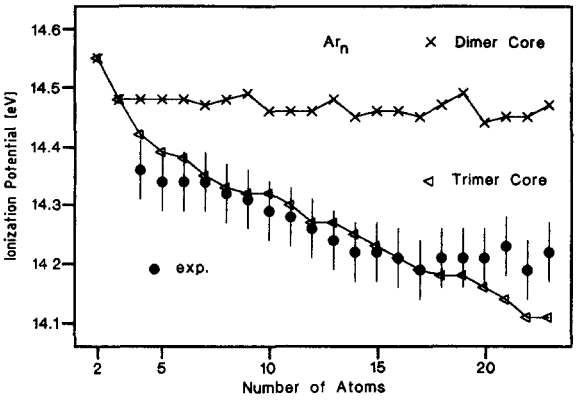

FIG. 7. Calculated ionization potentials of argon clusters (Ref. 17), assuming either a central dimer (×) or trimer (△) ion. The experimental data (○) follow closely the trimer curve up to $n \approx 17$.

ing energy of the electron hole trapping by the formation of Ar_3^+. This part is much smaller for the larger rare gases (Kr: 65%; Xe: 50%). The second part of the relaxation energy corresponds to the dipole induced binding energy of the layer around the localized charge, which plays a more important role for krypton and xenon. The different ratios of the covalent and induced dipole contributions to the binding do not arise from different dimer ion binding energies (Ar_2^+ :1.25 eV; Kr_2^+:1.15 eV; Xe_2^+: 0.99 eV).[22] In fact the dipole induced binding E_{dipole} is much stronger in the case of xenon compared to argon as it is proportional to the atomic polarizability. Consequently the difference between atomic IP and bulk work function is largest for xenon (Ar:1.85; Kr:2.10 eV; Xe:2.43 eV).[22] If we regard the cluster IP's from $n = 3$ to $n = 15$ as being proportional to E_{dipole} (the van der Waals binding energy of the neutrals may be neglected) we find the following correlation between the atomic polarizabilities and E_{dipole}:

	Ar		Kr	:	Xe
polarizability[26]	1	:	1.5	:	2.4
E_{dipole}	1	:	1.9	:	3.7

The dipole-induced binding of the neutral shell surrounding the central charge is more important for xenon cluster ions than for those of argon. [This has to be regarded as a qualitative argument only as the binding energy depends on polarizability (increasing from Ar to Xe) *and* on the atomic radius of the particles involved (decreasing from Ar to Xe) resulting in a net increase in polarization induced binding when going from Ar to Xe. E_{dipole}, on the other hand, is overestimated because of the neglect of interactions between the shell atoms and because of the finite size of the charge distribution.] We propose this as an explanation for the differences appearing in the mass spectra (Figs. 1(a) and 1(c)). A strong binding of the coordination shell to the central charge leads to the preference of spherical symmetry which is in this case equivalent to icosahedron geometry. For argon the tendency to form a sphere is weaker and various other effects may mainly influence the structures in the mass spectra, e.g., the geometrical deformation of the cluster ions caused by the formation of a central trimer ion ($n \leqslant 15$). In addition dynamical processes (fragmentation pattern) may also determine the intensities as has been shown recently.[27]

Finally we compare the measured IP's of the Ar_n clusters with calculations[17] (Fig. 7) The theoretical values are obtained by calculating the neutral and ionic binding energies at fixed temperatures. It is distinguished between a dimer and a trimer ion as the central charge carrier in the clusters. The IP's calculated with the assumption of a dimeric core are nearly equal for different n ($n = 3$–23). However, the data corresponding to a trimer ion charge carrier shows a decrease with n which is roughly parallel to the experimental values ($n \leqslant 15$).

This comparison of experimental and theoretical data support the assumption of a trimeric core in the size region $n \leqslant 15$. It also confirms the result of Levinger *et al.*,[18] who found an Ar_3^+ absorption line for argon cluster ions with $n \leqslant 15$. For larger cluster ions this resonance shifts and changes its shape. This explains the increasing deviation of the theoretical values from the measured ones above $n \approx 15$ in Fig. 7 as the calculation assume a central trimer ion for all n. Both experiments also support the results of diatomic-in-molecule calculations of Kuntz and Valldorf.[15] They found a linear Ar_3^+ inside the small argon clusters with $n \leqslant 14$. (The linearity of Ar_3^+ has independently been established by an MRD-CI calculation of Böhmer and Peyerimhoff[23].) For Ar_n^+ ($n \geqslant 14$) the positive charge begins to spread over a fourth atom and with increasing n a linear asymmetric tetramer ion is formed.

V. CONCLUSIONS

We have presented ion efficiency curves of Ar, Kr, and Xe clusters produced in a supersonic jet. Monochromatic synchrotron light served as the light source. The photoions are analyzed by their time of flight using the photoelectrons as start signals. Adiabatic IP's are determined and display a change of slope around $n = 15$ in the case of argon. This is explained by an effective screening of the outer atoms by the first coordination shell around a central trimer ion. The change of slope does not occur for krypton and xenon. The less effective screening may be caused by the higher polarizability of the neutral Kr and Ar atoms.

The examination of the IP development with increasing cluster size allows a rough estimate of that part of the bulk

relaxation energy which is due to the dipol-induced interaction. For xenon it is $\sim 50\%$ of the whole relaxation energy whereas in argon only $\sim 20\%$ is found. This is related to the higher polarizability of atomic xenon and causes a stronger preference of a spherical shape of these cluster ions. This may explain the observation of icosahedron shell closings in xenon cluster ion mass spectra which are only hardly detectable in argon mass spectra.

A comparison of calculated[17] Argon cluster IP's with measured ones support the conclusion of Levinger *et al.*[18] and also Kuntz and Valldorf,[15] who found experimental and theoretical evidence for Ar_3^+ as the central charge carrier in Ar_n^+ with $n \leqslant 15$.

ACKNOWLEDGMENTS

We wish to thank H.-U. Böhmer for making his unpublished calculations of Argon cluster IP's available to us. It is a pleasure to acknowledge very useful and stimulating discussions with K. H. Meiwes-Broer and H. O. Lutz. The technical assistance of Mr. Lehmann and the staff of BESSY is gratefully acknowledged.

[1]O. Echt, K. Sattler, and E. Recknagel, Phys. Rev. Lett. **47**, 1121 (1981).
[2]A. L. Mackay, Acta Crit. **15**, 916 (1967).
[3]O. Echt, in *Elemental and Molecular Clusters*, edited by G. Benedek, T. P. Martin and G. Pacchioni, Springer Series in Material Science 6 (Springer, Berlin, 1987), p. 263.
[4]H. Haberland, Surf. Sci. **156**, 305 (1985).
[5]T. D. Märk, Int. J. Mass Spectron. Ion Phys. **79**, 1 (1987).
[6]U. Buck and H. Meyer, Phys. Rev. Lett. 52, 109 (1984).
[7]D. Kreisle, O. Echt, M. Knapp, and E. Recknagel, Phys. Rev. A **33**, 768 (1986).
[8]P. G. Lethbridge and A. J. Stace, J. Chem. Phys. **89**, 4062 (1988).
[9]J. J. Saenz, J. M. Soler, and N. Garcia, Surf. Sci. **156**, 121 (1985).
[10]J. Jortner, D. Scharf, and U. Landman, in *Elemental and Molecular Clusters*, edited by G. Benedek, T. P. Martin, and G. Pacchioni, Springer Series in Material Science 6 (Springer, Berlin, 1987), p. 148.
[11]A. Ding and J. HeBlich, Chem. Phys. Lett. 94, **54** (1983).
[12]I. A. Harris, R. S. Kidwell, and J. A. Northby, Phys. Rev. Lett. **53**, 2390 (1984).
[13]E. D. Poliakoff, P. M. Dehmer, J. L. Dehmer, and R. Stockbauer, J. Chem. Phys. **76**, 5214 (1982).
[14]C. E. Klots, Z. Phys. D **5**, 83 (1987).
[15]P. J. Kuntz and J. Valldorf, Z. Phys. D **8**, 195 (1988).
[16]H.-U. Böhmer and S. D. Peyerimhoff, Z. Phys. D **8**, 91 (1988).
[17]H.-U. Böhmer and S. D. Peyerimhoff, Z. Phys. D **11**, 239 (1989). H.-U. Böhmer, Ph.D. thesis, Universität Bonn, 1987.
[18]N. E. Levinger, D. Ray, M. L. Alexander, and W. C. Lineberger, J. Chem. Phys. **89**, 5654 (1988).
[19]L. Cordis, G. Ganteför, J. HeBlich, and A. Ding, Z. Phys. D **3**, 323 (1986).
[20]E. Holub-Krappe, G. Ganteför, G. Bröker, and A. Ding, Z. Phys. D **10**, 319 (1988).
[21]J. Berkowitz, *Photoabsorption, Photoionization and Photoelectron Spectroscopy* (Academic, New York, 1979).
[22]N. Schwentner, E.-E. Koch, and J. Jortner, *Electronic Excitations in Condensed Rare Gases* (Springer, Berlin, 1985).
[23]H.-U. Böhmer and S. D. Peyerimhoff, Z. Phys. D **3**, 195 (1986), and References herein.
[24]P. M. Dehmer and J. L. Dehmer, J. Chem. Phys. **69**, 125 (1978).
[25]E. D. Poliakoff, P. M. Dehmer, J. L. Dehmer, and R. Stockbauer, J. Chem. Phys. **75**, 1568 (1981).
[26]A. A. Radzig and B. M. Smirnov, *Reference Data on Atoms, Molecules and Ions*, Springer Series in Chemical Physics 31 (Springer, Berlin, 1985).
[27]G. Ganteför, E. Holub-Krappe, G. Bröker, and A. Ding (to be published).